Loss of spatacsin impairs cholesterol trafficking and calcium homeostasis

Authors and affiliations:

Maxime Boutry[1-5,#], Alexandre Pierga[1-4], Raphaël Matusiak[1-4], Julien Branchu[1-4], Marc Houllegatte[1-5], Yoan Ibrahim[1-4], Elise Balse[6], Khalid-Hamid El Hachimi[1-5], Alexis Brice[1-4], Giovanni Stevanin[1-5], Frédéric Darios[1-4,*]

1: Sorbonne Université, UPMC Univ Paris 06, UMR S 1127, F-75013, Paris, France

2: Inserm, U1127, F-75013, Paris, France

3: CNRS, UMR 7225, F-75013, Paris, France

4: Institut du Cerveau et de la Moelle Epinière, ICM, F-75013, Paris, France

5: Ecole Pratique des Hautes Etudes, PSL Research University, Laboratoire de Neurogénétique, F-75013, Paris, France

6: Sorbonne Université, UPMC Univ Paris 06, UMR S 1166, F-75013 Paris, France

[#] Present address: Cell Biology Program, Hospital for Sick Children, Peter Gilgan Centre for Research and Learning, Toronto, ON, Canada

***** Corresponding author: Frédéric Darios

Institut du Cerveau et de la Moelle Epinière

INSERM U1127, CNRS UMR 7225, UPMC UMR S 1127

Hôpital de la Salpêtrière

47, Boulevard de l'Hôpital

F-75013 France

Tel: (+33) 1 57 27 46 52

Fax : (+33) 1 57 27 46 95

E-mail: frederic.darios@upmc.fr (F.D.)

Abstract:

Mutations in SPG11, leading to loss of spatacsin function, impair the formation of membrane tubules in lysosomes and cause the accumulation of lipids in lysosome compartment. However, the full nature of lipids accumulating in lysosomes and the physiological consequences of such accumulation are not known. Here we show that loss of spatacsin, but also downregulation of clathrin, inhibited the formation of tubules on late endosomes/lysosomes and prevented the clearance of cholesterol from this subcellular compartment. Using spatacsin-deficient cells, we evaluated the consequences of impaired cholesterol clearance from late endosomes/lysosomes. The accumulation of cholesterol in late endosomes/lysosomes led to lower cholesterol levels in the plasma membrane, enhancing the entry of extracellular calcium by store-operated calcium entry and increasing resting cytosolic calcium levels. Higher cytosolic calcium levels promoted the nuclear translocation of the master regulator of lysosomes TFEB. Downregulation of TFEB or decrease in resting calcium levels in absence of spatacsin partially corrected the formation of tubules and the accumulation of cholesterol in lysosomes, suggesting that spatacsin could be indirectly implicated in the formation of tubules. Our work reveals a homeostatic balance between cholesterol trafficking and cytosolic calcium levels and shows that loss of spatacsin impairs this homeostatic equilibrium.

Introduction

Mutations in the *SPG11* gene are responsible for a severe form of hereditary spastic paraplegia characterized by bilateral weakness, spasticity in the lower limbs, as well as ataxia or cognitive impairment (1, 2). Most mutations are truncating mutations, suggesting that the symptoms are due to loss of function of the *SPG11* product, spatacsin (3). Accordingly, knockout of *Spg11* in the mouse reproduces the main motor and cognitive symptoms observed in patients (4). Studies in SPG11 patient fibroblasts and in *Spg11* knockout mice suggested that loss of spatacsin led to impaired function of lysosomes (4-6). Lysosomes are organelles containing hydrolytic enzymes that notably fuse with endosomes or autophagosomes to allow degradation of their content. After the degradation step, new lysosomes can be reformed from the hybrid organelles (7, 8). Recycling of the lysosomal membrane after the termination of autophagy, known as autophagic lysosome recovery (ALR), relies on the formation of tubules on the lysosomes. This mechanism involves proteins that participate in membrane trafficking, such as clathrin and dynamin (9, 10), but it also relies on spatacsin (11).

Analysis of *Spg11* knockout mice showed that the loss of spatacsin function led to progressive accumulation of lipids in lysosomes, both in neuronal and non-neuronal cells (4). In particular, it was shown that loss of spatacsin led to lysosomal accumulation of glycosphingolipids in neuronal models (12). Most lipids such as triacylglycerols, phospholipids and gangliosides are degraded by the lysosomal hydrolases into their basic building blocks. The latter are then exported in the cytosol to be further degraded to fuel energy metabolism or can re-enter biosynthetic pathways (13). In contrast, cholesterol is not degraded in the endolysosomal pathway, but it is exported out of this subcellular compartment. It is redistributed to the membranes of other subcellular compartments, placing lysosomes at a crossroad of cholesterol metabolism (14). However, the molecular mechanisms by which cholesterol leaves late endosomes/lysosomes and reaches other subcellular compartments have been only partially characterized (15). Furthermore, alteration of cholesterol trafficking is associated with many pathological conditions (16). It is therefore important to explore the downstream consequences for cellular physiology of impaired cholesterol trafficking. Cholesterol has long been known to influence cellular calcium homeostasis, but little is known about the molecular mechanisms coupling change in cholesterol concentration to alterations of calcium signaling (17). Here, we show that the loss of spatacsin function and the associated inhibition of tubule formation in late endosomes/lysosomes leads to the accumulation of cholesterol in this compartment, due to its impaired export out of the organelle. This results in a

decrease in the level of plasma membrane cholesterol that disturbs intracellular calcium homeostasis. We demonstrate that the resulting modification in cytosolic calcium levels further enhances the impairment of lysosome tubulation and accumulation of cholesterol in late endosomes/lysosomes and that this process is TFEB-dependent.

Results:

The formation of tubules on lysosomes contributes to cholesterol clearance

The loss of spatacsin has been shown to impair lysosomal function (11, 12). We therefore analyzed the localization of lysosomes in control and spatacsin-deficient (*Spg11*$^{-/-}$) fibroblasts by LAMP1 immunostaining. *Spg11*$^{-/-}$ cells showed perinuclear accumulation of LAMP1-positive vesicles (Fig. 1A-B), a phenotype that has been linked to the accumulation of cholesterol in late endosomes and lysosomes (18, 19). We thus tested whether cholesterol accumulate in the late endosomes/lysosomes of *Spg11*$^{-/-}$ fibroblasts by monitoring intracellular localization of cholesterol with filipin, which stains free cholesterol (Fig. 1C), or the fluorescent probe derived from perfringolysin-O, GFP-D4 (Sup. Fig. 1A) (20). The mean fluorescence intensity of filipin staining of whole cells was the same in *Spg11*$^{+/+}$ and *Spg11*$^{-/-}$ fibroblasts (Fig. 1D), a result confirmed by the biochemical analysis of cellular cholesterol content (Sup. Fig. 1B). However, the proportion of cholesterol colocalized with late endosomes/lysosomes was significantly higher in *Spg11*$^{-/-}$ than control fibroblasts when monitored with filipin or GFP-D4 (Fig. 1E, Sup. Fig. 1C). Since mutations in *SPG11* cause neurodegeneration (3), we evaluated the impact of loss of spatacsin function on cholesterol distribution in neuronal models. Biochemical quantification showed that the amount of total cholesterol was similar in *Spg11*$^{+/+}$ and *Spg11*$^{-/-}$ neurons (Fig. 1F). We monitored whether cholesterol accumulates in the late endosomes/lysosomes of *Spg11*$^{-/-}$ neurons with the GFP-D4 probe (Fig. 1G). Consistent with data obtained in fibroblasts, the proportion of cholesterol colocalized with late endosomes/lysosomes was significantly higher in *Spg11*$^{-/-}$ than control neurons, suggesting that cholesterol distribution was impaired in neurons in the absence of spatacsin (Fig. 1H). Since the distribution of cholesterol, but not the total amount, was altered in the absence of spatacsin, we hypothesized that the trafficking of cholesterol could be disturbed.

We monitored the trafficking of fluorescently-labelled cholesterol. Control and *Spg11*$^{-/-}$ fibroblasts were incubated with low density lipoprotein (LDL) loaded with fluorescent cholesterol for two hours and chased for 24 hours. We quantified the colocalization of fluorescent cholesterol with LAMP1 at several time points. During the first four hours, the proportion of fluorescent cholesterol colocalized with LAMP1 increased, consistent with the internalization of LDL, and there was no difference in the internalization of cholesterol between *Spg11*$^{+/+}$ and *Spg11*$^{-/-}$ fibroblasts. At longer chase times, there was a progressive decrease in the colocalization of fluorescent cholesterol and LAMP1 in control cells,

consistent with the egress of cholesterol from late endosomes/lysosomes (21). In contrast, the proportion remained stable in *Spg11*$^{-/-}$ cells (Fig. 1I), suggesting that the efflux of cholesterol from late endosomes/lysosomes was altered in the absence of spatacsin.

Spatacsin participates in the initiation of tubule formation on lysosomes (11). Accordingly, we observed that *Spg11*$^{-/-}$ fibroblasts contained fewer lysosomes with tubules than *Spg11*$^{+/+}$ fibroblasts under basal condition when they were transfected with a vector expressing LAMP1-mCherry and analyzed by live imaging (Sup Fig. 2A-B). We tested whether the formation of tubules contributed to cholesterol clearance from lysosomes using siRNA to downregulate the clathrin heavy chain (Fig. 2A), a protein essential for the initiation of tubule formation on late endosomes/lysosomes (9). Downregulation of the clathrin heavy chain in wild-type fibroblasts significantly decreased the number of tubules emanating from lysosomes and increased the proportion of cholesterol colocalized with the LAMP1-positive compartment under basal condition (Fig. 2B-C). Pulse-chase experiments of LDL loaded with fluorescent cholesterol showed that the efflux of cholesterol from late endosomes/lysosomes decreased when clathrin heavy chain was downregulated (Sup Fig. 2C). The scission of lysosome tubules requires dynamin (10), a binding partner of spatacsin (12). The inhibition of dynamin by dynasore increased the proportion of cholesterol colocalized with late endosomes/lysosomes in control, but not in *Spg11*$^{-/-}$ fibroblasts (Fig. 2D). These data suggest that spatacsin and dynamin cooperate in a same pathway to clear cholesterol from late endosomes/lysosomes. Overall, these data suggest that the formation of tubules on lysosomes contributes to the clearance of cholesterol from lysosomes.

We investigated whether lysosomal tubules are used for cholesterol trafficking by transfecting fibroblasts with a vector expressing LAMP1-mCherry and incubating them with LDL loaded with fluorescent cholesterol for two hours in the presence of U18666a. This compound promotes the strong accumulation of cholesterol in late endosomes and lysosomes (22). Twenty minutes after U18666a washout, which allows cholesterol egress from lysosomes, live imaging showed the fluorescent cholesterol to be localized to lysosomal tubules (Fig. 2E). Occasionally, tubules fission gave rise to new vesicles containing cholesterol (Fig. 2E), suggesting that tubulation in late endosomes/lysosomes is involved in cholesterol trafficking.

Inhibition of lysosome tubulation decreases cholesterol levels in the plasma membrane

In cells, cholesterol levels are high in the plasma membrane, intermediate in late endosome/lysosomes, and low in the endoplasmic reticulum (ER) (23). We investigated whether the accumulation of cholesterol in late endosomes/lysosomes changes its concentration in the plasma membrane by staining cholesterol in the plasma membrane of live cells using the probe GFP-D4. Cholesterol levels in the plasma membrane were significantly lower in *Spg11*$^{-/-}$ than control cells (Fig. 3A-B). We confirmed this result by determining total and plasma membrane cholesterol levels by an enzymatic assay. The total amount of cholesterol was the same in *Spg11*$^{-/-}$ and *Spg11*$^{+/+}$ cells (Fig. Sup 1B), but it was lower in the plasma membrane of *Spg11*$^{-/-}$ than *Spg11*$^{+/+}$ cells (Fig. 3C). Similarly, the inhibition of tubule formation in late endosomes/lysosomes by downregulation of clathrin heavy chain or dynasore treatment led to the accumulation of cholesterol in late endosomes/lysosomes at the expense of the plasma membrane (Fig 2, Fig 3D and 3E). Overall, these results show that impaired trafficking of cholesterol out of late endosomes/lysosomes due to alterations in the formation of tubules results in decreased levels of cholesterol in the plasma membrane.

Lower levels of cholesterol in the plasma membrane increase store-operated calcium entry

We then investigated the consequences of impaired trafficking of cholesterol from lysosomes to the plasma membrane by analyzing cells deficient in spatacsin, which is required for the initiation of tubule formation (11). On electron microcopy preparations, the loss of spatacsin significantly increased the number and size of the contacts between ER and the plasma membrane (Fig. 4A-C). Such close contacts play a role in various cellular functions and notably regulate transfer of lipids between the membranes, or homeostasis of calcium (24, 25). Upon depletion of the intracellular calcium store of the ER, the ER calcium sensor STIM1 oligomerizes and interacts with the plasma membrane calcium channel Orai1, forming close contacts between the ER and the plasma membrane and allowing the import of extracellular calcium to restore normal intracellular calcium homeostasis (25). This mechanism is known as store-operated calcium entry (SOCE). We analyzed the proximity of the ER calcium sensor STIM1 and the plasma membrane by total internal reflection fluorescence (TIRF) in cells transfected with a vector expressing STIM1-mCherry. TIRF microscopy performed on fibroblasts under basal conditions confirmed that the proportion of the plasma membrane in close contact with the ER calcium sensor STIM1 was higher in *Spg11*$^{-/-}$ than control cells (Fig. 4D-E).

Levels of cholesterol in the plasma membrane regulate SOCE (26, 27). We therefore tested whether lower levels of cholesterol in the plasma membrane, caused by the loss of spatacsin, altered SOCE. We treated fibroblasts in Ca^{2+}-free medium with the SERCA inhibitor thapsigargin to deplete the ER calcium store and trigger SOCE. We then added 2 mM calcium in the extracellular medium and calcium import was measured using the cytosolic calcium probe Fura-2. *Spg11*$^{-/-}$ cells imported more extracellular calcium than *Spg11*$^{+/+}$ cells (Fig. 4F), suggesting that the loss of spatacsin promoted SOCE under basal conditions.

We then investigated whether the increased SOCE observed in the absence of spatacsin was due to lower levels of cholesterol in the plasma membrane. We increased plasma membrane cholesterol levels by exposing *Spg11*$^{-/-}$ fibroblasts for one hour to methyl-β-cyclodextrin loaded with cholesterol (Suppl. Fig. 3A and B). This restored normal SOCE in *Spg11*$^{-/-}$ fibroblasts (Fig. 4G), suggesting that cholesterol depletion from the plasma membrane due to impaired lysosomal tubulation is responsible for the increase in SOCE when spatacsin function is lost.

Cholesterol depletion in the plasma membrane increases cytosolic calcium levels

SOCE promotes the entry of extracellular calcium into the cytosol that is normally taken up by the ER (25, 28). We monitored whether the increased SOCE due to the loss of spatacsin modified cytosolic calcium levels in resting cells. Cytosolic calcium levels were slightly, but significantly, higher in *Spg11*$^{-/-}$ than *Spg11*$^{+/+}$ fibroblasts (Fig. 5A). We tested whether this increase in cytosolic calcium was a consequence of increased SOCE by reducing extracellular calcium levels to 0.4 mM by adding EGTA to the culture medium for one hour. Under these conditions, SOCE decreased markedly in both *Spg11*$^{+/+}$ and *Spg11*$^{-/-}$ fibroblasts (data not shown) along with resting cytosolic calcium levels (Fig. 5A). We confirmed this result by downregulating the expression of STIM1 by transfecting fibroblasts with specific siRNA (Fig. 5B). Downregulation of STIM1 decreased SOCE and restored normal cytosolic calcium levels in *Spg11*$^{-/-}$ cells (Fig. 5B-C), demonstrating that enhanced SOCE increases cytosolic calcium levels in the absence of spatacsin. Finally, we restored normal cytosolic calcium levels when we increased cholesterol levels in the plasma membrane of *Spg11*$^{-/-}$ fibroblasts (Suppl. Fig. 3), suggesting that the increase in SOCE, caused by lower plasma membrane cholesterol levels, is responsible for the alteration of cytosolic calcium levels (Fig. 5D).

High cytosolic calcium levels impair lysosome tubulation and contribute to the accumulation of cholesterol in lysosomes in a TFEB-dependent manner

Among other cellular functions, the entry of extracellular calcium by SOCE has been proposed to regulate the nuclear translocation of TFEB (29), which is a major regulator of lysosome function (30). We monitored the amount of nuclear TFEB, which represents the transcriptionally active protein (30), in *Spg11*$^{-/-}$ and *Spg11*$^{+/+}$ fibroblasts. The amount of nuclear TFEB was significantly higher in *Spg11*$^{-/-}$ than *Spg11*$^{+/+}$ fibroblasts, whereas cytosolic levels of TFEB were not significantly different (Fig. 6A). Decreasing cytosolic calcium levels using the intracellular chelator EGTA-AM or by lowering extracellular calcium levels decreased the amount of nuclear TFEB in *Spg11*$^{-/-}$ fibroblasts, suggesting that higher SOCE in *Spg11*$^{-/-}$ fibroblasts is responsible for the nuclear translocation of the transcription factor (Fig. 6A). Since TFEB regulates many lysosome functions, we wondered whether the higher levels of nuclear TFEB due to higher cytosolic calcium levels could regulate the formation of tubules of late endosomes/lysosomes and modulate the cholesterol content in this compartment.

We decreased SOCE by downregulating STIM1 or reducing extracellular free Ca^{2+} levels. These treatments partially restored tubule formation in the absence of spatacsin (Fig. 6B and Suppl. Fig. 4A). Similarly, treatment with the intracellular calcium chelator EGTA-AM, to decrease cytosolic calcium levels, increased the number of lysosomes with tubules in *Spg11*$^{-/-}$ fibroblasts (Fig. 6C). We tested whether these effects where mediated by TFEB by downregulating its expression using siRNA, leading to lower levels of TFEB in both the cytoplasm and nucleus (Fig 6D). Downregulation of TFEB in *Spg11*$^{-/-}$ fibroblasts restored the number of lysosomes with tubules (Fig. 6E). Overall, these data suggest that altered calcium homeostasis impairs the formation of tubules on lysosomes in the absence of spatacsin in a TFEB-dependent manner.

We showed that tubule formation is required for the clearance of cholesterol from lysosomes (Fig. 1). We thus investigated whether treatment that restores the formation of tubules in the absence of spatacsin also has an effect on cholesterol accumulation in late endosomes/lysosomes. Decreasing SOCE by reducing the extracellular calcium concentration or downregulating STIM1 expression corrected the accumulation of cholesterol observed in lysosomes in *Spg11*$^{-/-}$ fibroblasts (Fig. 6F, Suppl. Fig. 4B). Similarly, decreasing cytosolic calcium levels with EGTA-AM decreased cholesterol levels in late endosomes/lysosomes in *Spg11*$^{-/-}$ fibroblasts (Fig. 6G) and *Spg11*$^{-/-}$ neurons (Sup. Fig. 5). Downregulation of TFEB in *Spg11*$^{-/-}$ fibroblasts also decreased the proportion of cholesterol in late

endosomes/lysosomes (Fig. 6H), suggesting that increased cytosolic calcium levels contributed to the accumulation of cholesterol in a TFEB-dependent manner.

We also showed that the accumulation of cholesterol in late endosomes/lysosomes slightly decreases cholesterol levels in the plasma membrane (Fig. 3). We reasoned that treatment that restores the distribution of cholesterol in late endosomes/lysosomes in *Spg11*$^{-/-}$ fibroblasts should also restore normal levels of cholesterol in the plasma membrane. Inhibiting SOCE via STIM1 downregulation indeed corrected cholesterol levels in the plasma membrane of *Spg11*$^{-/-}$ fibroblasts (Fig. 6I), showing that dysregulation of calcium homeostasis contributed to the observed alterations in cholesterol trafficking. This demonstrates that impaired calcium homeostasis due to the accumulation of cholesterol in late endosomes/lysosomes contributed to the maintenance or enhancement of the imbalanced cholesterol distribution.

Discussion

Loss of spatacsin leads to accumulation of lipids in lysosomes, both in neuronal and non-neuronal cells (4), but the mechanisms underlying the accumulation of lipids in this compartment are unknown. Here we show that spatacsin is implicated in the trafficking of cholesterol and demonstrate that alteration of this trafficking pathway has functional consequences for the plasma membrane, calcium homeostasis, affecting lysosome function.

Cholesterol is an essential constituent of cellular membranes, but is unevenly distributed within subcellular compartments (23, 31). The lipid composition of membranes, including the amount of cholesterol, affects their biological function (32). The mechanisms that regulate cholesterol transport between subcellular compartments thus appear to be critical for cellular functions (14). The transport of cholesterol out of lysosomes requires the proteins Niemann Pick Type C (NPC) 1 and 2 that likely allow cholesterol to be integrated in the lysosomal membrane (14, 23, 33). However, the dissection of mechanisms allowing cholesterol transport is complicated by the co-existence of vesicular transport of cholesterol (21) and non-vesicular trafficking of cholesterol at the levels of contact sites between lysosomes and other subcellular compartments (31, 34).

The formation of tubules on lysosomes requires clathrin, spatacsin, and dynamin. These proteins are involved in the recycling of lysosome membranes after the termination of autophagy (9-11). Although autophagic lysosome recovery occurs after the termination of autophagy, we show here that this machinery is also used to clear cholesterol from late endosomes/lysosomes by tubulation under basal conditions. Accordingly, downregulation of spatacsin was shown to decrease the formation of tubules on late endosomes/lysosomes under basal conditions (11). The accumulation of cholesterol in late endosomes/lysosomes due to the inhibition of tubulation leads to lower cholesterol levels in the plasma membrane. shRNA screening consistently identified spatacsin as a regulator of cholesterol trafficking from lysosomes toward the plasma membrane (35). The formation of tubules could give rise to vesicles that may participate in the vesicular trafficking of cholesterol from late endosomes/lysosomes to the plasma membrane. The mechanism that regulates such trafficking is not clear, but it may involve Rab8a and myosin5b, as previously observed (21).

Changes in the concentration of cholesterol in the plasma membrane enhance the entry of extracellular calcium by SOCE and leads to higher cytosolic calcium levels, which could contribute to alter calcium signaling (17). Cholesterol has been shown to inhibit the activity of the Orai1 channel (26),

consistent with the higher SOCE observed when plasma membrane cholesterol levels are lower. A recent study showed that the entry of calcium by SOCE promotes nuclear translocation of the master lysosomal gene TFEB, promoting its transcriptional activity (29). In accordance with these results, we observed increased nuclear translocation of TFEB in absence of spatacsin. Decreasing calcium entry or cytosolic calcium levels was sufficient to restore normal nuclear TFEB levels in the absence of spatacsin. Thus, changes in plasma membrane composition could indirectly modulate lysosomal function through calcium-dependent regulation of TFEB. Downregulation of TFEB or treatments that compensated for the deregulation of calcium homeostasis were able to partially restore the formation of tubules on late endosomes/lysosomes, in the absence of spatacsin, and restore cholesterol homeostasis. The interdependence of cholesterol trafficking and calcium homeostasis highlights a homeostatic equilibrium in which the impairment of cholesterol clearance from lysosomes modifies plasma membrane composition, thus affecting calcium homeostasis and lysosomal cholesterol content in a TFEB-dependent manner. The compensatory role of the downregulation of TFEB or the decrease in cytosolic calcium levels on the formation of tubules in late endosomes/lysosomes suggest that spatacsin could be indirectly implicated in the formation of tubules or that alternative mechanisms could compensate for the absence of spatacsin. However, the exact role of spatacsin in the maintenance of the homeostasis of calcium and cholesterol still need to be elucidated.

Our data support the hypothesis that the loss of spatacsin leads to similar impairment of cholesterol and calcium homeostasis both in non-neuronal cells and in neurons. Hereditary spastic paraplegia SPG11 is characterized by neuronal death in various brain regions (4, 36). The persistent deregulation of cholesterol distribution could lead to a slight modification of calcium homeostasis. Calcium plays a central role in cellular physiology and neuronal transmission (37) and a persistent change in cytosolic calcium levels could explain the behavioral alterations that were observed in *Spg11*$^{-/-}$ mice long before neurodegeneration occurred (4). Alternatively, alteration in calcium homeostasis in absence of spatacsin, could also contribute, in the long term, to neurodegeneration (38).

In conclusion, we demonstrate that loss of spatacsin function impairs trafficking of cholesterol leading to a strong alteration of cellular homeostasis that could contribute to neuronal dysfunction. Atlastin that is mutated in the SGP3 form of HSP has also been proposed to modulate SOCE and lipid metabolism (39). It would be interesting to investigate the role of atlastin in the distribution of cholesterol. Conversely, alterations of cholesterol trafficking in endosomes and lysosomes have also been described

in models of Alzheimer's disease (40), and impaired distribution of cholesterol seems to play a crucial role in neurodegeneration in the case of Alzheimer's disease (41). It may be informative to test whether the deregulation of cholesterol homeostasis in late endosomes in this disease also induce an alteration of cellular homeostasis that could contribute to persistent and deleterious impairment of lysosomal function.

Materials and Methods

Antibodies and chemicals: Thapsigargin, filipin, $CaCl_2$, EDTA, and cholesterol were purchased from Sigma. EGTA-AM was purchased from Thermo Scientific. Dynasore was purchased from Abcam. Antibodies used in the study were: mouse anti-α-tubulin (Abcam); rat anti-LAMP1 (Clone 1D4B, Development Studies Hybridoma Bank), mouse anti clathrin heavy chain (BD Biosciences), mouse anti-STIM1 (Cell Signalling), rabbit anti-TFEB (Proteintech), and rabbit anti-histone H3 (Cell Signalling). For immunoblotting, the secondary antibodies were conjugated to horseradish peroxidase (Jackson Laboratories) or fluorochromes (IR-dye 800 or IR-dye 680; LI-COR). Secondary antibodies used for immunofluorescence were purchased from Thermo Scientific.

Mouse embryonic fibroblast cultures: *Spg11*$^{-/-}$ mice were described previously (4). Mouse embryonic fibroblasts (MEFs) were prepared using E14.5 embryos obtained from the breeding of heterozygous mice. After removing the head and inner organs, the body was minced with a razor blade and incubated in 0.25% trypsin/EDTA (Gibco) for 15 min at 37°C. Cells were dissociated and grown in DMEM medium (Gibco) supplemented with 10% FBS and 1% penicillin/streptomycin. All experiments were performed between passages 4 to 6. At least three independent preparations of fibroblasts were used for each experiment.

Primary cultures of cortical neurons: Cortices of E14.5 embryos were mechanically dissociated in HBSS medium and plated at 25,000 neurons/cm2 on poly-D-Lysine (250 µg/ml) coated glass coverslips. The neurons were grown in Neurobasal medium supplemented with 2% B27 (Gibco), 2mM L-glutamine and 2% fetal bovine serum. Half of the medium was changed every two days and neurons were fixed after six days *in vitro* with 4% paraformaldehyde.

Electron microscopy: Mice were anaesthetized and sacrificed by intracardiac perfusion with a solution of 4% paraformaldehyde (PFA) in 0.1 M phosphate buffer at pH7.4. Samples from the frontal cortex were fixed in 1% glutaraldehyde in the same buffer, post-fixed in 2% osmium tetroxyde, dehydrated, and embedded in Araldite. Ultrathin sections were stained with uranyl acetate and lead citrate and examined using a Hitashi transmission electron microscope. Images were analyzed using ImageJ.

Calcium Imaging: Cells grown in Lab-Tek™ (Nunc) were washed with HCSS buffer (120 mM NaCl, 5.4 mM KCl, 0.8 mM $MgCl_2$, 15 mM glucose, and 20 mM Hepes [pH 7.4]) and incubated with 2.5 µM Fura-2-AM (Life Technologies) for 30 min at room temperature in the dark. Cells were washed with HCSS and incubated 15 min at room temperature to allow Fura-2 de-esterification. Images were recorded with a Nikon Eclipse Ti-E inverted microscope, with excitation of Fura 2-AM loaded cells alternately at 340 and 380 nm. Emission at 510 nm was recorded. Conversion of Fura-2 ratios into cytosolic calcium concentrations was performed as previously described (42).

Plasmids and Transfection: LAMP1-mCherry was obtained from Addgene (#45147). STIM1-mcherry was obtained from R. Lewis (43). Fibroblasts were transfected with the Neon transfection system (Invitrogen), according to the manufacturer's instructions, using the following parameters: 1350 V, 30 ms, and one pulse. For overexpression studies, we used 0.5 µg DNA per 50.10^3 cells and the analysis was performed 24 h after transfection. For silencing studies, 50.10^3 cells were transfected with 1 pmol siRNA (Invitrogen) and analyzed 48 h later. The sequence of siRNA targeting STIM1 was 5'-GCAAGGAUGUUAUAUUUGATT-3', that targeting clathrin heavy chain, 5'-CAUUGUCUGUGAUCGGUUUTT-3', and that targeting TFEB, 5'-CAACCUAAUUGAGAGAAGATT-3'.

Immunofluorescence: After fixation with 4% PFA, cells were incubated with PBS containing 10 mM NH_4Cl for 10 min at 22°C to quench autofluorescence. Cells were incubated with a solution of 5% BSA/ 0.1% Triton X-100 in PBS for 30 min at 22°C and then with primary antibodies in 5% BSA/0.1% Triton X-100 in PBS overnight at 4°C. After washing, the cells were incubated with the secondary antibodies for 45 min at room temperature and mounted in Prolong Gold reagent (Thermo Scientific). Images were acquired with a Zeiss upright microscope equipped with a Plan-APOCHROMAT objective (63X; NA: 1.4), allowing acquisition of optical section images (Apotome 2 microscope).

Lysosome positioning: The position of lysosomes was assessed using ImageJ and MATLAB (MathWorks©) software. Signals from the nucleus (DAPI) and lysosomes (LAMP1) from an optical section were acquired with an Apotome 2 microscope. The centroid of the nucleus was determined using the DAPI signal and centroids of each lysosome were determined as the pixel with the highest

intensity for each LAMP1-positive vesicle. The distance between lysosome centroids and the nucleus centroid was calculated. The results were expressed as the relative distance to the nucleus with 100 being the distance between the nucleus and the farthest lysosome.

Live-cell imaging: The formation of tubules in late endosomes/lysosomes was followed by live imaging of cells expressing LAMP1-mcherry at 37°C and 5% CO2 using a Leica DMi8 microscope equipped with a Yokogawa Confocal Spinning Disk module. Cells were chosen randomly, with the only criterion being LAMP1-mCherry levels sufficiently high to detect lysosomal tubules.

Cholesterol staining: Cells were fixed with 4% PFA for 30 min at 22°C. They were then incubated with filipin (50 µg/ml) in PBS supplemented with 10% FBS for 2 h at room temperature in the dark, without prior permeabilization. Cells were then processed for immunostaining when required. Cholesterol levels were quantified as the mean grey value using ImageJ. Colocalization of cholesterol staining with lysosomes was quantified using ImageJ on randomly chosen images of cultured fibroblasts. First, we created a mask corresponding to LAMP1 staining using the automatic threshold in Image J. The mask was copied to the corresponding fluorescence image of cholesterol. We quantified the total intensity of cholesterol fluorescence in the lysosome mask and expressed it as the percentage of total cholesterol fluorescence in every cell. A preparation of domain D4 of prefringolysin O fused to GFP (GFP-D4) was produced and purified as previously described (44). Labelling of total cholesterol was performed by incubating fixed and permeabilized cells with 20 µg/ml recombinant GFP-D4 for 20 min at 22°C. Cholesterol of the outer leaflet of the plasma membrane was labeled by incubating live cells for 15 min at 22°C with 20 µg/mL GFP-D4 diluted in PBS containing 2 mM $CaCl_2$ and 0.8 mM $MgCl_2$. Cells were then fixed with 4% paraformaldehyde for 20 min and processed for imaging.

Cholesterol measurement: Cells cultured in 60-mm petri dishes were harvested and lysed by incubation in 100 mM NaCl, 10 mM Tris HCl pH 7.4, 1 mM EGTA, 2 mM $MgCl_2$, 1% Triton X-100, and Halt™ Protease Inhibitor Cocktail (Thermo Scientific) for 30 min at 4°C. The total cellular cholesterol concentration was measured using the Amplex® Red Cholesterol Assay Kit (Thermo Scientific). The values were normalized to total cellular protein concentration, which was determined by BCA assay (Thermo Scientific).

The cholesterol content of the plasma membrane was measured using a protocol modified from (35). Briefly, cells were extensively washed with ice-cold assay buffer (310 mM sucrose, 1mM MgSO4, 0.5mM Sodium phosphate [pH 7.4]) and then incubated with or without 1 U/mL cholesterol oxidase for 3 min at room temperature. The buffer was removed and the cells washed once with ice-cold assay buffer. Cells were lysed and the cholesterol concentration measured as described above. The plasma membrane cholesterol concentration was calculated by subtracting the amount of intracellular cholesterol (cells incubated with cholesterol oxidase) from the total amount of cholesterol (cells incubated in the absence of cholesterol oxidase). The values were normalized to total cellular protein concentration determined by BCA assay.

Cholesterol trafficking: Unlabeled LDL (1 mg) from human plasma (Thermo Scientific) was incubated with 50 nmol cholesterol (Top-Fluor cholesterol, Avanti Polar Lipids) for 2 h at 40°C and dialyzed overnight in PBS supplemented with 1mM EDTA. LDL-deprived serum was prepared as described previously (45). Cells were cultured in medium prepared with LDL-deprived serum for 24 h. Cholesterol trafficking was monitored by adding LDL complexed with Top-Fluor Cholesterol to the cells followed by incubation for 2 h. Cells were washed with culture medium and fixed with 4% PFA after various times of incubation in LDL-free medium.

Cholesterol loading of plasma membranes: Methyl-β-cyclodextrin (150 mg, MBCD, Sigma) was mixed with 5 mg cholesterol (Sigma) in 1 ml PBS and sonicated for 5 min (45% duty cycle, Branson Sonifier 250). Cells were incubated for 1 h at 37°C with 1.5mg MBCD/50 µg cholesterol/mL in serum-free DMEM medium.

Western blot analysis: Downregulation of clathrin heavy chain or STIM1 was evaluated by lysing cells in 100 mM NaCl, 10 mM Tris HCl pH 7.4, 1 mM EGTA, 2 mM $MgCl_2$, 1% Triton X-100, and Halt™ Protease Inhibitor Cocktail (Thermo Scientific) for 15 min at 4°C. Lysates were cleared by a 15-min centrifugation at 16,000 x g at 4°C. The subcellular localization of TFEB was evaluated by preparing the cells as described previously (46). Protein concentration was determined with the BCA assay kit. Western blots were performed as described previously (47). Signals were visualized with a

chemiluminescence substrate (SuperSignal West Dura) or acquired with an Odyssey ClX (Li-COR) instrument. Signal intensities were quantified using ImageJ software.

Total internal reflection fluorescence (TIRF) microscopy: TIRF experiments were performed on fibroblasts transfected with vectors expressing STIM1-mCherry, using a previously described protocol (48). Analyses were performed using ImageJ software. The TIRF signal was obtained by thresholding and the area containing the TIRF signal normalized to the surface for each cell.

Statistics and data analysis: All values are presented as the means ± SEM within each group. All statistical tests were performed using GraphPad Prism 6 and the tests are described in the figure legends. $P < 0.05$ was considered to be statistically significant.

Ethical approval

The care and treatment of animals followed European legislation (N° 2010/63/UE) and national (Ministère de l'Agriculture, France) guidelines for the detention, use, and ethical treatment of laboratory animals. All experiments on animals were approved by the local ethics committee (Ce5/2012/045 approval number) and conducted by authorized personnel.

Acknowledgments

We thank Phenoparc, IGenSeq, Celis, and the ICM.quant facilities of the Institut du Cerveau et de la Moelle Épinière for their contributions. The 1D4B monoclonal antibody was obtained from the Developmental Studies Hybridoma Bank (University of Iowa, Department of Biology, IA 52242). This work was supported by the “Investissements d’avenir” program grants [ANR-10-IAIHU-06] and [ANR-11-INBS-0011] and received funding from the Verum Foundation (to A.B. and G.S.), the French Agency for Research (ANR) (to G.S.), the *GIS-Maladies Rares* Foundation (to G.S.), the *Fondation Roger de Spoelberch* (to A.B.), and the European Union with the ANR (to A.B., Seventh Framework Programme - FP7, Omics call; to G.S., the E-Rare programme) and the European Research Council (European Research Council Starting [grant No 311149] to F.D.). M.B. received a fellowship from the French Ministry of Research (Doctoral School ED3C). A.P. received an ARDoC fellowship (17012953) from the Région Ile de France (Doctoral School ED3C).

Conflict of Interest Statement

The authors have no conflict of interest to declare.

Author contributions

M.B., A.B., G.S. and F.D. conceived and designed the experiments.

M.B., A.P., R.M. J.B., M.H., Y.I., E.B., K.H.E.H. and F.D. performed the experiments.

M.B., A.P., R.M. and F.D. analyzed the data.

M.B. and F.D. wrote the paper with comments of all co-authors.

References

1 Stevanin, G. *et al.* (2008) Mutations in SPG11 are frequent in autosomal recessive spastic paraplegia with thin corpus callosum, cognitive decline and lower motor neuron degeneration. *Brain*, **131**, 772-784.
2 Paisan-Ruiz, C. *et al.* (2008) SPG11 mutations are common in familial cases of complicated hereditary spastic paraplegia. *Neurology*, **70**, 1384-1389.
3 Stevanin, G. *et al.* (2007) Mutations in SPG11, encoding spatacsin, are a major cause of spastic paraplegia with thin corpus callosum. *Nat Genet*, **39**, 366-372.
4 Branchu, J. *et al.* (2017) Loss of spatacsin function alters lysosomal lipid clearance leading to upper and lower motor neuron degeneration. *Neurobiol Dis*, **102**, 21-37.
5 Varga, R.E. *et al.* (2015) In Vivo Evidence for Lysosome Depletion and Impaired Autophagic Clearance in Hereditary Spastic Paraplegia Type SPG11. *PLoS genetics*, **11**, e1005454.
6 Renvoise, B. *et al.* (2014) Lysosomal abnormalities in hereditary spastic paraplegia types SPG15 and SPG11. *Ann Clin Transl Neurol*, **1**, 379-389.
7 Bright, N.A. *et al.* (1997) Dense core lysosomes can fuse with late endosomes and are re-formed from the resultant hybrid organelles. *J Cell Sci*, **110 (Pt 17)**, 2027-2040.
8 Yu, L. *et al.* (2010) Termination of autophagy and reformation of lysosomes regulated by mTOR. *Nature*, **465**, 942-946.
9 Rong, Y. *et al.* (2012) Clathrin and phosphatidylinositol-4,5-bisphosphate regulate autophagic lysosome reformation. *Nat Cell Biol*, **14**, 924-934.
10 Schulze, R.J. *et al.* (2013) Lipid droplet breakdown requires dynamin 2 for vesiculation of autolysosomal tubules in hepatocytes. *J Cell Biol*, **203**, 315-326.
11 Chang, J. *et al.* (2014) Spastic paraplegia proteins spastizin and spatacsin mediate autophagic lysosome reformation. *J Clin Invest*, **124**, 5249-5262.
12 Boutry, M. *et al.* (2018) Inhibition of Lysosome Membrane Recycling Causes Accumulation of Gangliosides that Contribute to Neurodegeneration. *Cell Rep*, **23**, 3813-3826.
13 Schulze, H. *et al.* (2009) Principles of lysosomal membrane degradation: Cellular topology and biochemistry of lysosomal lipid degradation. *Biochimica et biophysica acta*, **1793**, 674-683.
14 Thelen, A.M. and Zoncu, R. (2017) Emerging Roles for the Lysosome in Lipid Metabolism. *Trends Cell Biol*, **27**, 833-850.
15 Luo, J. *et al.* (2017) Routes and mechanisms of post-endosomal cholesterol trafficking: A story that never ends. *Traffic*, **18**, 209-217.
16 Soffientini, U. and Graham, A. (2016) Intracellular cholesterol transport proteins: roles in health and disease. *Clin Sci (Lond)*, **130**, 1843-1859.
17 Mackrill, J.J. (2011) Oxysterols and calcium signal transduction. *Chem Phys Lipids*, **164**, 488-495.
18 Li, X. *et al.* (2016) A molecular mechanism to regulate lysosome motility for lysosome positioning and tubulation. *Nat Cell Biol*, **18**, 404-417.
19 Rocha, N. *et al.* (2009) Cholesterol sensor ORP1L contacts the ER protein VAP to control Rab7-RILP-p150 Glued and late endosome positioning. *J Cell Biol*, **185**, 1209-1225.
20 Ohno-Iwashita, Y. *et al.* (2004) Perfringolysin O, a cholesterol-binding cytolysin, as a probe for lipid rafts. *Anaerobe*, **10**, 125-134.
21 Kanerva, K. *et al.* (2013) LDL cholesterol recycles to the plasma membrane via a Rab8a-Myosin5b-actin-dependent membrane transport route. *Dev Cell*, **27**, 249-262.
22 Lu, F. *et al.* (2015) Identification of NPC1 as the target of U18666A, an inhibitor of lysosomal cholesterol export and Ebola infection. *Elife*, **4**.
23 Mesmin, B. *et al.* (2013) Insights into the mechanisms of sterol transport between organelles. *Cell Mol Life Sci*, **70**, 3405-3421.
24 Saheki, Y. and De Camilli, P. (2017) Endoplasmic Reticulum-Plasma Membrane Contact Sites. *Annu Rev Biochem*, **86**, 659-684.

25 Prakriya, M. and Lewis, R.S. (2015) Store-Operated Calcium Channels. *Physiol Rev*, **95**, 1383-1436.
26 Derler, I. *et al.* (2016) Cholesterol modulates Orai1 channel function. *Sci Signal*, **9**, ra10.
27 Pacheco, J. *et al.* (2016) A cholesterol-binding domain in STIM1 modulates STIM1-Orai1 physical and functional interactions. *Sci Rep*, **6**, 29634.
28 Smyth, J.T. *et al.* (2010) Activation and regulation of store-operated calcium entry. *J Cell Mol Med*, **14**, 2337-2349.
29 Zhu, Z.D. *et al.* (2018) SOCE induced calcium overload regulates autophagy in acute pancreatitis via calcineurin activation. *Cell Death Dis*, **9**, 50.
30 Settembre, C. *et al.* (2012) A lysosome-to-nucleus signalling mechanism senses and regulates the lysosome via mTOR and TFEB. *EMBO J*, **31**, 1095-1108.
31 Ikonen, E. (2018) Mechanisms of cellular cholesterol compartmentalization: recent insights. *Current opinion in cell biology*, **53**, 77-83.
32 Harayama, T. and Riezman, H. (2018) Understanding the diversity of membrane lipid composition. *Nat Rev Mol Cell Biol*, **19**, 281-296.
33 Kwon, H.J. *et al.* (2009) Structure of N-terminal domain of NPC1 reveals distinct subdomains for binding and transfer of cholesterol. *Cell*, **137**, 1213-1224.
34 Holthuis, J.C. and Menon, A.K. (2014) Lipid landscapes and pipelines in membrane homeostasis. *Nature*, **510**, 48-57.
35 Chu, B.B. *et al.* (2015) Cholesterol transport through lysosome-peroxisome membrane contacts. *Cell*, **161**, 291-306.
36 Denora, P.S. *et al.* (2016) Motor neuron degeneration in spastic paraplegia 11 mimics amyotrophic lateral sclerosis lesions. *Brain*, **139**, 1723-1734.
37 Gleichmann, M. *et al.* (2011) Homeostatic disinhibition in the aging brain and Alzheimer's disease. *J Alzheimers Dis*, **24**, 15-24.
38 Mattson, M.P. (2007) Calcium and neurodegeneration. *Aging Cell*, **6**, 337-350.
39 Li, J. *et al.* (2017) Atlastin regulates store-operated calcium entry for nerve growth factor-induced neurite outgrowth. *Sci Rep*, **7**, 43490.
40 Yang, D.S. *et al.* (2014) Defective macroautophagic turnover of brain lipids in the TgCRND8 Alzheimer mouse model: prevention by correcting lysosomal proteolytic deficits. *Brain*, **137**, 3300-3318.
41 Arenas, F. *et al.* (2017) Intracellular Cholesterol Trafficking and Impact in Neurodegeneration. *Front Mol Neurosci*, **10**, 382.
42 Grynkiewicz, G. *et al.* (1985) A new generation of Ca2+ indicators with greatly improved fluorescence properties. *J Biol Chem*, **260**, 3440-3450.
43 Luik, R.M. *et al.* (2006) The elementary unit of store-operated Ca2+ entry: local activation of CRAC channels by STIM1 at ER-plasma membrane junctions. *J Cell Biol*, **174**, 815-825.
44 Abe, M. and Kobayashi, T. (2017) Dynamics of sphingomyelin- and cholesterol-enriched lipid domains during cytokinesis. *Methods Cell Biol*, **137**, 15-24.
45 Goldstein, J.L. *et al.* (1983) Receptor-mediated endocytosis of low-density lipoprotein in cultured cells. *Methods Enzymol*, **98**, 241-260.
46 Medina, D.L. *et al.* (2017) Methods to Monitor and Manipulate TFEB Activity During Autophagy. *Methods Enzymol*, **588**, 61-78.
47 Esteves, T. *et al.* (2014) Loss of association of REEP2 with membranes leads to hereditary spastic paraplegia. *Am J Hum Genet*, **94**, 268-277.
48 Eichel, C.A. *et al.* (2016) Lateral Membrane-Specific MAGUK CASK Down-Regulates NaV1.5 Channel in Cardiac Myocytes. *Circ Res*, **119**, 544-556.

Figure Legends

Figure 1. The loss of spatacsin (*Spg11*$^{-/-}$) promotes the accumulation of cholesterol in late endosomes/lysosomes.

A. Immunostaining of *Spg11*$^{+/+}$ and *Spg11*$^{-/-}$ fibroblasts with the late endosome/lysosome marker LAMP1. Nuclei are stained with DAPI. White lines indicate the cell periphery. Scale bar: 10 µm.

B. Distribution of late endosomes/lysosomes in *Spg11*$^{+/+}$ and *Spg11*$^{-/-}$ fibroblasts. The maximum distance between particles and the nucleus was fixed at 100 for each cell. Late endosomes/lysosomes cluster more around the nuclei of *Spg11*$^{-/-}$ than *Spg11*$^{+/+}$ fibroblasts. The graph shows the mean ± SEM. N = 65 cells for at least three independent experiments. Two-way ANOVA followed by Holm-Sidak multiple comparison test: *** $p < 0.0001$; **$p<0.01$; *$p<0.05$.

C. Staining of cholesterol with filipin and late endosomes/lysosomes by the marker LAMP1 in *Spg11*$^{+/+}$ and *Spg11*$^{-/-}$ fibroblasts. Insets show a higher magnification of the zone highlighted by a white square. Scale bar: 10 µm.

D. Quantification of the intensity of filipin staining of whole cells showing no significant difference in the total amount of cholesterol in *Spg11*$^{+/+}$ and *Spg11*$^{-/-}$ fibroblasts. The graph shows the mean ± SEM. N > 85 cells for at least three independent experiments. T-test: $p = 0.83$.

E. Quantification of the amount of filipin staining colocalized with the marker LAMP1, showing more cholesterol in late endosomes/lysosomes in *Spg11*$^{-/-}$ than *Spg11*$^{+/+}$ fibroblasts. The graph shows the mean ± SEM. N > 85 cells for at least three independent experiments. T-test: ***$p < 0.0001$.

F. Biochemical quantification of total cholesterol levels in *Spg11*$^{+/+}$ (N=7) and *Spg11*$^{-/-}$ (N=6) neurons. Mann-Whitney test: $p = 0.63$.

G. Staining of cholesterol with GFP-D4 probe and immunostaining of the late endosome/lysosome marker LAMP1 in *Spg11*$^{+/+}$ and *Spg11*$^{-/-}$ primary cortical neurons. Scale bar: 5 µm.

H. Quantification of the amount of GFP-D4 staining colocalized with the marker LAMP1, showing more cholesterol in late endosomes/lysosomes in *Spg11*$^{-/-}$ than *Spg11*$^{+/+}$ neurons. The graph shows the mean ± SEM. N > 110 cells for at least three independent experiments. T-test: ***$p < 0.001$.

I. Quantification of the amount of Top-Fluor cholesterol colocalized with the marker LAMP1 in *Spg11*$^{+/+}$ and *Spg11*$^{-/-}$ fibroblasts over time. Fibroblasts were incubated with LDL loaded with Top-Fluor cholesterol for 2 h, rinsed, and analyzed after various chase times. Colocalization of Top-Fluor cholesterol with LAMP1 increased during the first 4 h in *Spg11*$^{+/+}$ and *Spg11*$^{-/-}$ fibroblasts. Then, the colocalization of Top-Fluor cholesterol with LAMP1 decreased in *Spg11*$^{+/+}$ but not *Spg11*$^{-/-}$ fibroblasts. The graph shows the mean ± SEM. N > 95 cells analyzed in at least three independent experiments. Two-way ANOVA followed by Holm-Sidak multiple comparison test: *** $p < 0.0001$.

Figure 2. **Inhibition of tubule formation in late endososmes/lysosomes causes the accumulation of cholesterol**

A. Western blot showing the downregulation of clathrin heavy chain (CHC) in wild-type mouse embryonic fibroblasts transfected with siRNA targeting CHC.
B. Quantification of the number of LAMP1-positive tubules in wild-type fibroblasts transfected with a control siRNA or a siRNA that downregulates CHC and expressing LAMP1 fused to mCherry, analyzed by live imaging. The graph shows the mean ± SEM. N > 58 cells analyzed in three independent experiments. T-test: ***$p = 0.0004$.
C. Quantification of the amount of filipin staining colocalized with the LAMP1 marker in fibroblasts transfected with a control siRNA or a siRNA that downregulates CHC. Downregulation of CHC resulted in a higher amount of cholesterol in late endosomes/lysosomes. The graph shows the mean ± SEM. N > 78 cells analyzed in three independent experiments. T-test: ***$p = 0.0002$.
D. Two-hour treatment of fibroblasts with the dynamin inhibitor dynasore (40 µM) induces the accumulation of cholesterol in *Spg11*$^{+/+}$ but not *Spg11*$^{-/-}$ fibroblasts. The graph shows the mean ± SEM. N > 78 cells analyzed in three independent experiments. Two-way ANOVA followed by Holm-Sidak multiple comparison test: *$p = 0.037$, **$p = 0.0098$.
E. Live imaging of fibroblasts expressing LAMP1-mCherry and loaded with fluorescent cholesterol coupled to LDL. Note the presence of fluorescent cholesterol in tubules emanating from LAMP1-positive late endosomes/lysosomes (asterisk). Arrowheads point to a lysosomal tubule undergoing fission. Scale bar: 2 µm.

Figure 3. The inhibition of tubule formation on late endosomes/lysosomes lowers cholesterol content in the plasma membrane

A. Staining of live fibroblasts with the probe GFP-D4, which allows staining of the plasma membrane cholesterol only. Scale bar: 10 µm.

B. Quantification of the intensity of GFP-D4 staining performed on live *Spg11*$^{+/+}$ and *Spg11*$^{-/-}$ fibroblasts, showing a lower level of plasma membrane cholesterol in *Spg11*$^{-/-}$ than *Spg11*$^{+/+}$ fibroblasts. The graphs show the mean ± SEM. N > 95 cells analyzed in at least three independent experiments. T-test: ***p < 0.0001.

C. Biochemical quantification of the proportion of cholesterol present in the plasma membrane in *Spg11*$^{+/+}$ and *Spg11*$^{-/-}$ fibroblasts, showing a lower level of plasma membrane cholesterol in *Spg11*$^{-/-}$ than *Spg11*$^{+/+}$ fibroblasts. N = 6 independent assays. Wilcoxon paired test: *p = 0.031.

D. Quantification of the intensity of GFP-D4 staining performed on live fibroblasts transfected with control siRNA or siRNA targeting CHC. Downregulation of CHC decreases the amount of cholesterol in the plasma membrane. The graph shows the mean ± SEM. N > 100 cells analyzed in two independent experiments. T-test: ***p < 0.0001.

E. Quantification of the intensity of GFP-D4 staining performed on live fibroblasts treated with dynasore (40 µM, 2 h). Inhibition of dynamin decreases the amount of cholesterol in the plasma membrane. The graph shows the mean ± SEM. N > 80 cells analyzed in three independent experiments. T-test: ***p = 0.0062.

Figure 4: The depletion of plasma membrane cholesterol promotes higher store-operated calcium entry

A. Electron micrograph of neurons in the cortex of a two-month-old *Spg11*$^{-/-}$ mouse, showing close contact between the endoplasmic reticulum (ER) and plasma membrane (PM). False colors highlight the various cellular compartments. Scale bar: 250 nm.

B-C. Quantification of contacts between the ER and plasma membrane, defined as the zone where the distance between the two membranes is lower than 30 nm. **B.** Quantification of the mean length of

individual contacts between the ER and plasma membrane in the cortex of two-month-old *Spg11*$^{-/-}$ or *Spg11*$^{+/+}$ mice. **C.** Quantification of the percentage of the plasma membrane in close contact with the ER in the cortex of two-month-old *Spg11*$^{-/-}$ or *Spg11*$^{+/+}$ mice. The graphs represent he mean ± SE. N > 23 cells analyzed in two independent mice for each group. T-test: ***p < 0.0001.

D. *Spg11*$^{-/-}$ or *Spg11*$^{+/+}$ mouse embryonic fibroblasts transfected with vectors expressing STIM1-mCherry imaged by epifluorescence or total internal reflection microscopy (TIRF). Scale bar: 10 µm.

E. Quantification of the percentage of the cellular area with STIM1-mCherry staining detected by TIRF microscopy, indicating close contact between STIM1-mCherry and the plasma membrane. The graph shows the mean ± SEM. N > 60 cells for at least three independent experiments. T-test: ***p < 0.0001.

F. Evaluation of extracellular calcium import by SOCE. Cytosolic calcium was measured with Fura-2 in the absence of extracellular calcium. The ER calcium store was depleted with thapsigargin, 2mM $CaCl_2$ added to the extracellular medium, and the increase in cytosolic calcium measured with Fura-2, allowing the quantification of SOCE. The graph shows the mean ± SEM. N > 35 cells for three independent experiments.

G. Increasing cholesterol levels in the plasma membrane with methyl-b-cyclodextrin (MBCD) loaded with cholesterol decreases store-operated calcium entry in *Spg11*$^{-/-}$ fibroblasts, measured by the addition of 2 mM extracellular calcium after a 10 min treatment with thapsigargin. The graph shows he mean ± SEM. N > 60 cells for three independent experiments.

Figure 5. High store-operated calcium entry in the absence of spatacsin increases cytoplasmic calcium levels.

A. Quantification of cytosolic calcium levels in *Spg11*$^{+/+}$ and *Spg11*$^{-/-}$ fibroblasts in normal medium or medium supplemented with EGTA to lower the extracellular calcium to 0.4 mM. The graphs represent the mean ± SEM. N > 159 cells for at least three independent experiments. Two-way ANOVA: ***p < 0.0001.

B. Downregulation of STIM1 strongly abrogates store-operated calcium entry in *Spg11*$^{+/+}$ and *Spg11*$^{-/-}$ fibroblasts. The graphs show the mean ± SEM. N > 55 cells for at least three independent experiments.

Insert: Western blot showing the downregulation of STIM1 in *Spg11*$^{+/+}$ and *Spg11*$^{-/-}$ fibroblasts transfected with siRNA directed against STIM1. Representative image of at least three independent experiments.

C. Downregulation of STIM1 decreases the levels of cytosolic calcium in *Spg11*$^{-/-}$ fibroblasts to those measured in *Spg11*$^{+/+}$ fibroblasts. The graph shows the mean ± SEM. N > 190 cells analyzed in at least three independent experiments. Two-way ANOVA: *p < 0.02.

D. Treatment of *Spg11*$^{+/+}$ or *Spg11*$^{-/-}$ fibroblasts with methyl-β-cyclodextrin (MBCD) loaded with cholesterol for 1 h restores normal cytosolic calcium levels in *Spg11*$^{-/-}$ cells. The graph shows the mean ± SEM. N > 70 cells for three independent experiments. Two-way ANOVA followed by the Holm-Sidak multiple comparison test: ** p = 0.0012, ***p = 0.0005.

Figure 6. High cytosolic calcium levels cause accumulation of cholesterol in late endosomes/lysosomes in the absence of spatacsin.

A. Western blot of TFEB in cytosolic and nuclear fractions of *Spg11*$^{+/+}$ and *Spg11*$^{-/-}$ fibroblasts cultured for 2 h in normal medium or medium containing either 0.4 mM CaCl2 or 0.5 µM EGTA-AM. Lower panel: quantification of the amount of TFEB normalized to the levels of α-tubulin (Cytosol) and Histone H3 (Nuclei). The graph shows the mean ± SEM. N > 4 independent experiments. One-way ANOVA: *p < 0.05, **p < 0.01.

B-C. Quantification of the number of LAMP1-positive tubules in *Spg11*$^{+/+}$ and *Spg11*$^{-/-}$ fibroblasts expressing LAMP1-mCherry, analyzed by live imaging. The number of LAMP1-positive tubules was lower in *Spg11*$^{-/-}$ than *Spg11*$^{+/+}$ fibroblasts. The number of tubules increased in *Spg11*$^{-/-}$ fibroblasts when they were transfected with a siRNA that downregulates STIM1 (B) or incubated in a medium containing 0.5 µM EGTA-AM for 1 h (C). The graphs show the mean ± SEM. B: N > 60 cells analyzed in four independent experiments. Two-way ANOVA followed by the Holm-Sidak multiple comparison test: *p = 0.034, ***p < 0.0001. C: N > 60 cells analyzed in four independent experiments. Two-way ANOVA followed by the Holm-Sidak multiple comparison test: *p = 0.030, ***p < 0.0001.

D. Western blots of TFEB in cytosolic and nuclear fractions of *Spg11*$^{+/+}$ and *Spg11*$^{-/-}$ fibroblasts transfected with control siRNA or a specific siRNA that downregulates TFEB.

E. Quantification of the number of LAMP1-positive tubules in *Spg11*$^{+/+}$ and *Spg11*$^{-/-}$ fibroblasts transfected with control siRNA or siRNA that downregulates TFEB. The graph shows the mean ± SEM. N > 60 cells analyzed in four independent experiments. Two-way ANOVA followed by the Holm-Sidak multiple comparison test: ***p < 0.0001.

F. Downregulation of STIM1 decreases the amount of cholesterol colocalized with a late endosome/lysosome marker in *Spg11*$^{-/-}$ fibroblasts. The graph shows the mean ± SEM. N > 95 cells analyzed in three independent experiments. Two-way ANOVA followed by the Holm-Sidak multiple comparison test: ***p < 0.001.

G. Lowering intracellular calcium levels with EGTA-AM (0.5µM, 1 h) decreases the amount of cholesterol colocalized with a late endosome/lysosome marker in *Spg11*$^{-/-}$ fibroblasts. The graph shows the mean ± SEM. N > 45 cells analyzed in three independent experiments. Two-way ANOVA followed by the Holm-Sidak multiple comparison test: ***p < 0.001.

H. Downregulation of TFEB decreases the amount of cholesterol colocalized with a late endosome/lysosome marker in *Spg11*$^{-/-}$ fibroblasts. The graph shows the mean ± SEM. N > 45 cells analyzed in three independent experiments. Mann Whitney test: *p < 0.05.

I. Quantification of plasma membrane cholesterol with the probe GFP-D4, performed on live *Spg11*$^{+/+}$ and *Spg11*$^{-/-}$ fibroblasts, showing that downregulation of STIM1 restores normal levels of cholesterol in the plasma membrane in *Spg11*$^{-/-}$ fibroblasts. The graph shows the mean ± SEM. N > 180 cells analyzed in three independent experiments. Two-way ANOVA followed by the Holm-Sidak multiple comparison test ***p < 0.0001.

Supplementary data

Supplementary Figure 1. The loss of spatacsin promotes the accumulation of cholesterol in late endosomes/lysosomes.

A. Staining of cholesterol with the probe GFP-D4 and late endosomes/lysosomes by the marker LAMP1 in *Spg11*$^{+/+}$ and *Spg11*$^{-/-}$ fibroblasts. Scale bar: 10 µm.

B. Biochemical quantification of total cholesterol levels in *Spg11*$^{+/+}$ and *Spg11*$^{-/-}$ fibroblasts. N = 11 in six independent experiments. Mann-Whitney test: p = 0.86

C. Quantification of the amount of GFP-D4 staining colocalized with the marker LAMP1, showing a higher amount of cholesterol in late endosomes/lysosomes in *Spg11*$^{-/-}$ than *Spg11*$^{+/+}$ fibroblasts. The graph shows the mean ± SEM. N > 45 cells analyzed in three independent experiments. T-test: ***p < 0.0001.

Supplementary Figure 2. The formation of tubules on lysosomes contributes to the clearance of cholesterol

A. Live imaging of *Spg11*$^{+/+}$ and *Spg11*$^{-/-}$ fibroblasts transfected with a vector expressing LAMP1 fused to mCherry. Note the presence of tubules (arrowheads in insets) emanating from late endosomes/lysosomes in *Spg11*$^{+/+}$ fibroblasts. Scale bar: 10 µm.

B. Quantification of the number of LAMP1-positive tubules in *Spg11*$^{+/+}$ and *Spg11*$^{-/-}$ fibroblasts. The graph shows the mean ± SEM. N > 200 cells analyzed in three independent experiments. T-test: ***p < 0.0001.

C. Quantification of the amount of Top-Fluor cholesterol colocalized with the LAMP1 marker in control fibroblasts transfected with control siRNA or siRNA downregulating CHC. Fibroblasts were incubated with LDL loaded with Top-Fluor cholesterol for 2 h, rinsed, and analyzed after various chase times. The graph shows the mean ± SEM. N > 45 cells analyzed in three independent experiments. Two-way ANOVA followed by Holm-Sidak multiple comparison test: *** p < 0.0001.

Supplementary Figure 3. Loading of the plasma membrane with cholesterol

A. Live imaging of plasma-membrane cholesterol in cells stained with the probe GFP-D4, showing that loading of fibroblasts with methyl-β-cyclodextrin (MBCD) coupled with cholesterol increases the amount of plasma membrane cholesterol. Scale bar: 10 µm.

B. Relative amount of plasma membrane cholesterol monitored by staining with the probe GFP-D4 in live cells. The graph shows the mean ± SEM. N > 55 cells analyzed in three independent experiments. Two-way ANOVA followed by the Holm-Sidak multiple comparison test: ***p < 0.0001.

Supplementary Figure 4. Decreasing the extracellular calcium concentration restores the formation of tubules and normal cholesterol levels in lysosomes in *Spg11*$^{-/-}$ fibroblasts.

A. Quantification of the number of LAMP1-positive tubules in *Spg11*$^{+/+}$ and *Spg11*$^{-/-}$ fibroblasts expressing LAMP1-mCherry, analyzed by live imaging. The number of LAMP1-positive tubules was lower in *Spg11*$^{-/-}$ than *Spg11*$^{+/+}$ fibroblasts in a medium containing 2 mM $CaCl_2$. The number of tubules in *Spg11*$^{-/-}$ fibroblasts increased when they were incubated in a medium containing 0.4 mM $CaCl_2$ for 1 h. The graph shows the mean ± SEM. N > 45 cells analyzed in three independent experiments. Two-way ANOVA followed by the Holm-Sidak multiple comparison test: *p = 0.042, ***p < 0.0001.

B. Incubation of fibroblasts in a medium containing 0.4 mM $CaCl_2$ for 1 h decreases the amount of cholesterol colocalized with a late endosome/lysosome marker in *Spg11*$^{-/-}$ fibroblasts. The graphs represent the mean ± SEM. N > 65 cells analyzed in at least three independent experiments. Two-way ANOVA followed by the Holm-Sidak multiple comparison test: ***p < 0.001.

Supplementary Figure 5. Buffering cytosolic calcium restores normal cholesterol levels in lysosomes in *Spg11*$^{-/-}$ primary cortical neurons. Incubation of neurons in a medium containing 0.5µM

EGTA-AM for 1 h decreases the amount of cholesterol colocalized with a late endosome/lysosome marker in *Spg11*$^{-/-}$ neurons. The graphs represent the mean ± SEM. N > 110 cells analyzed in at least three independent experiments. Two-way ANOVA followed by the Holm-Sidak multiple comparison test: **p < 0.01.

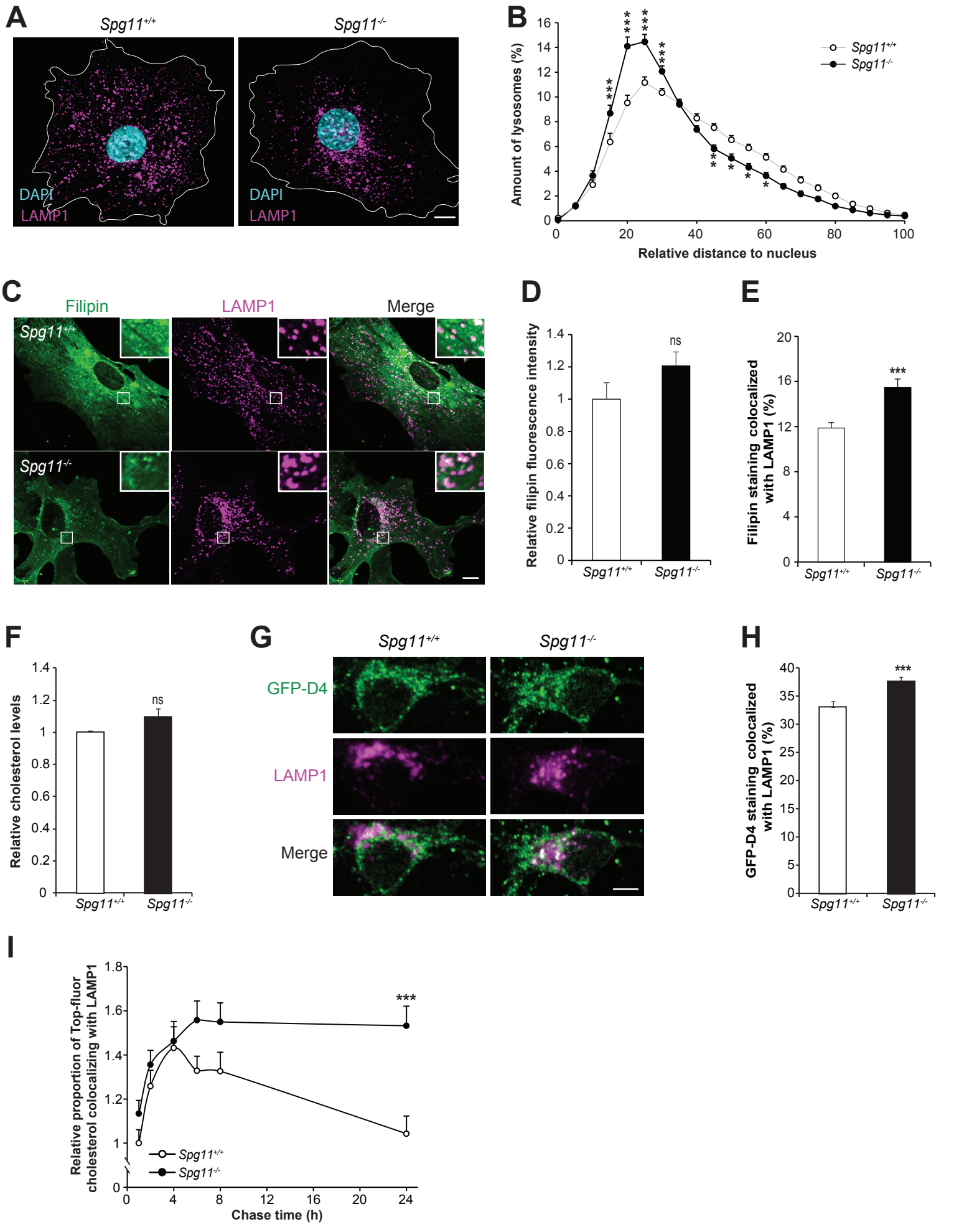

Boutry et al. figure 2

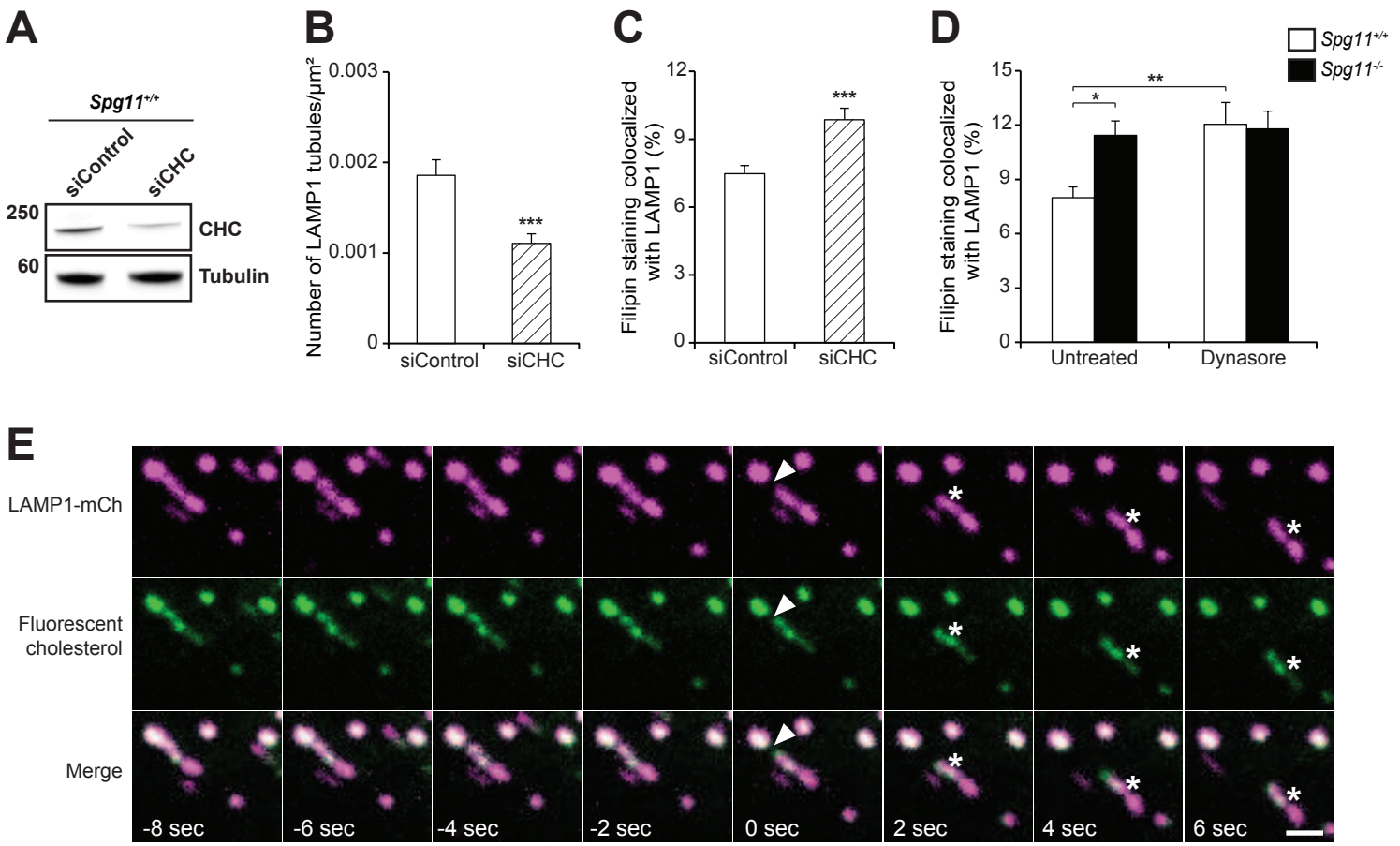

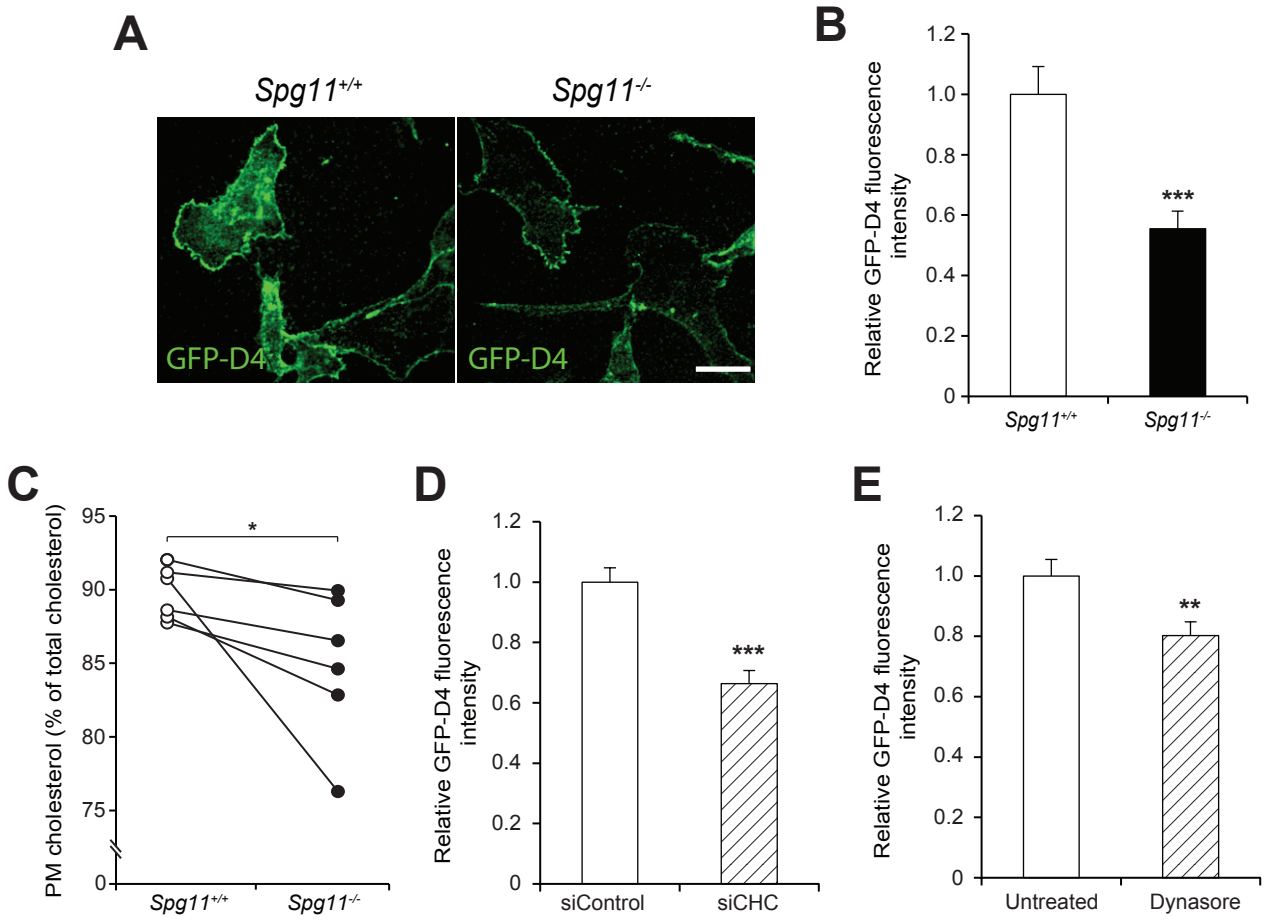

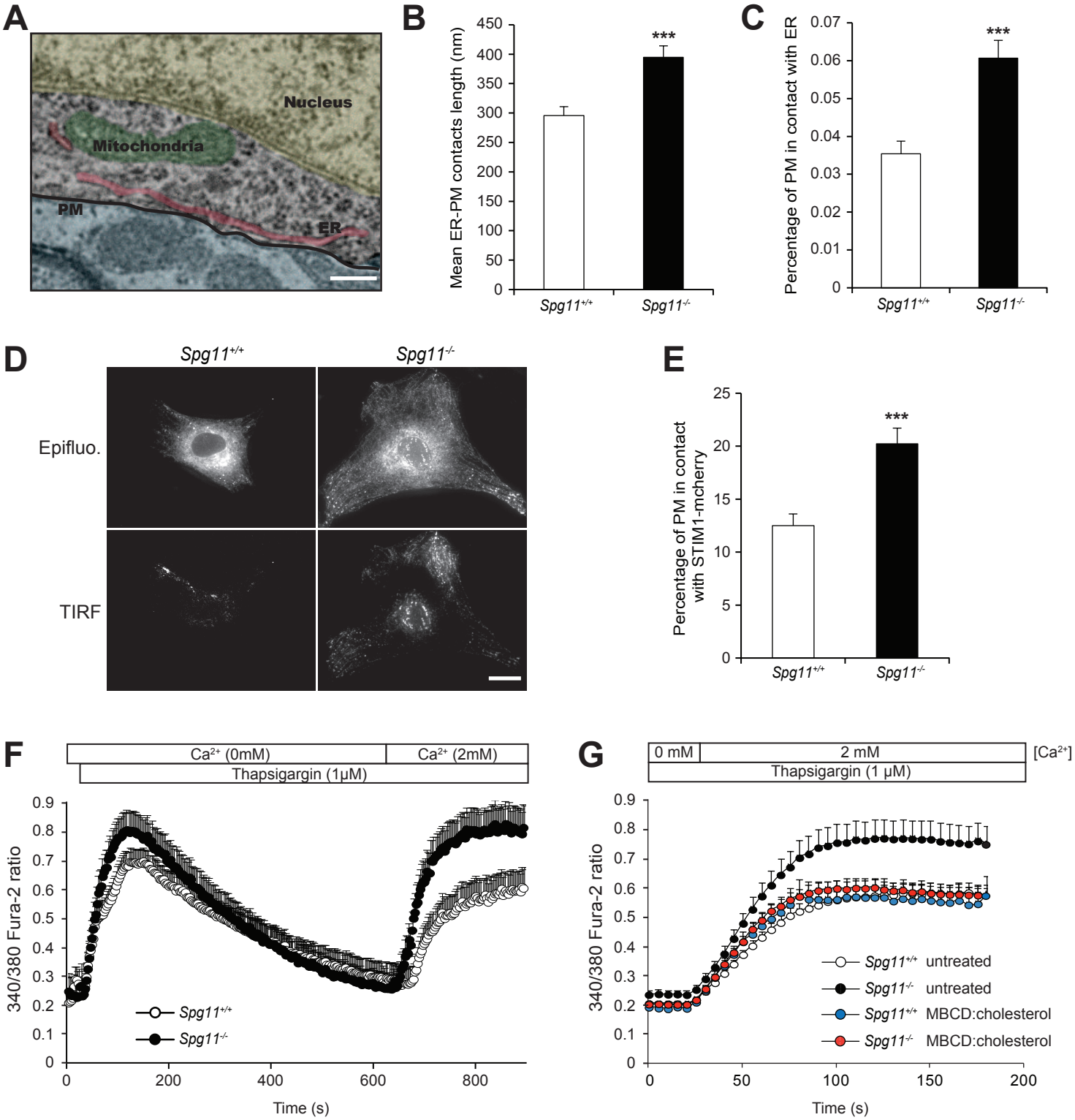

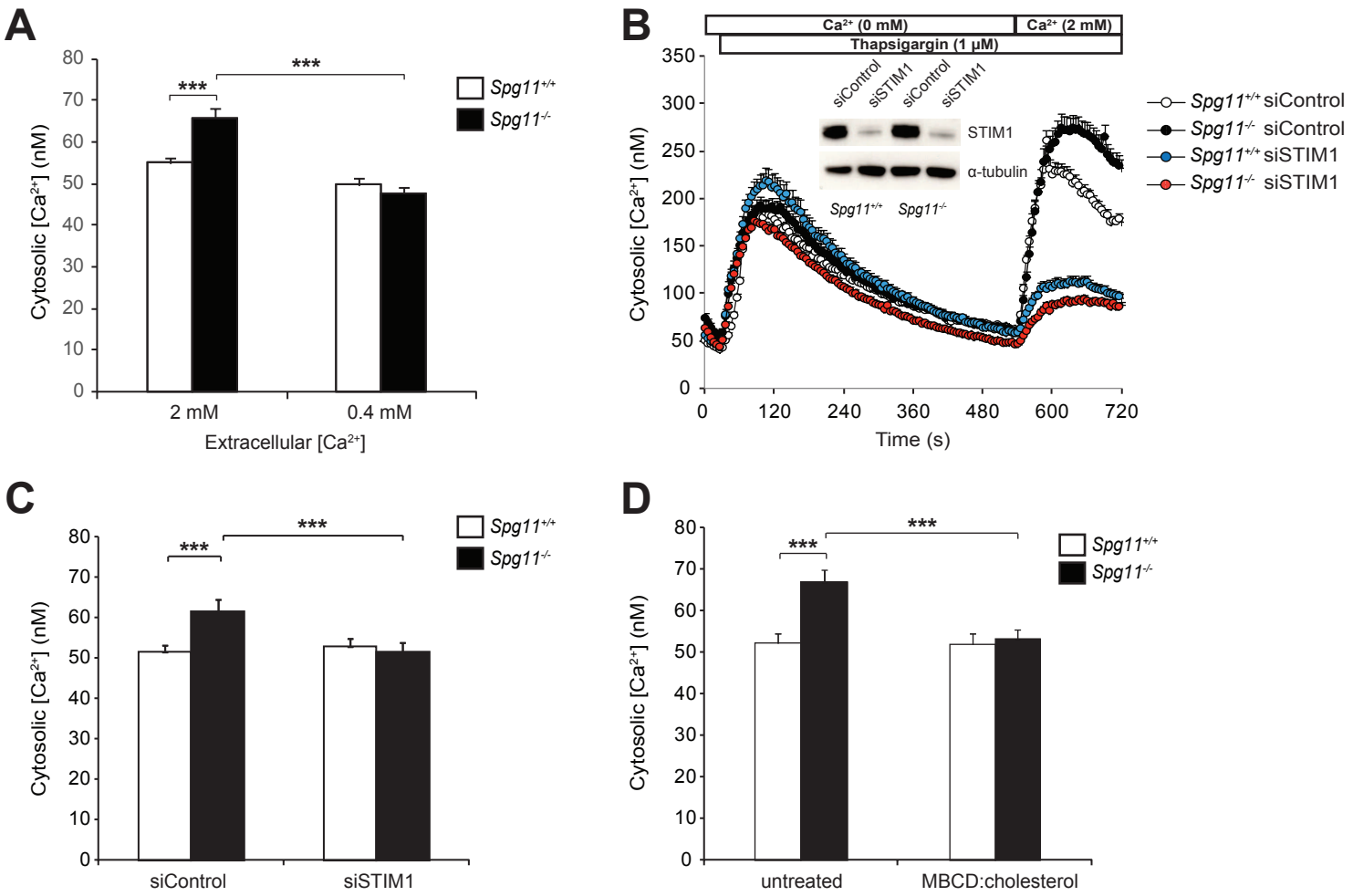

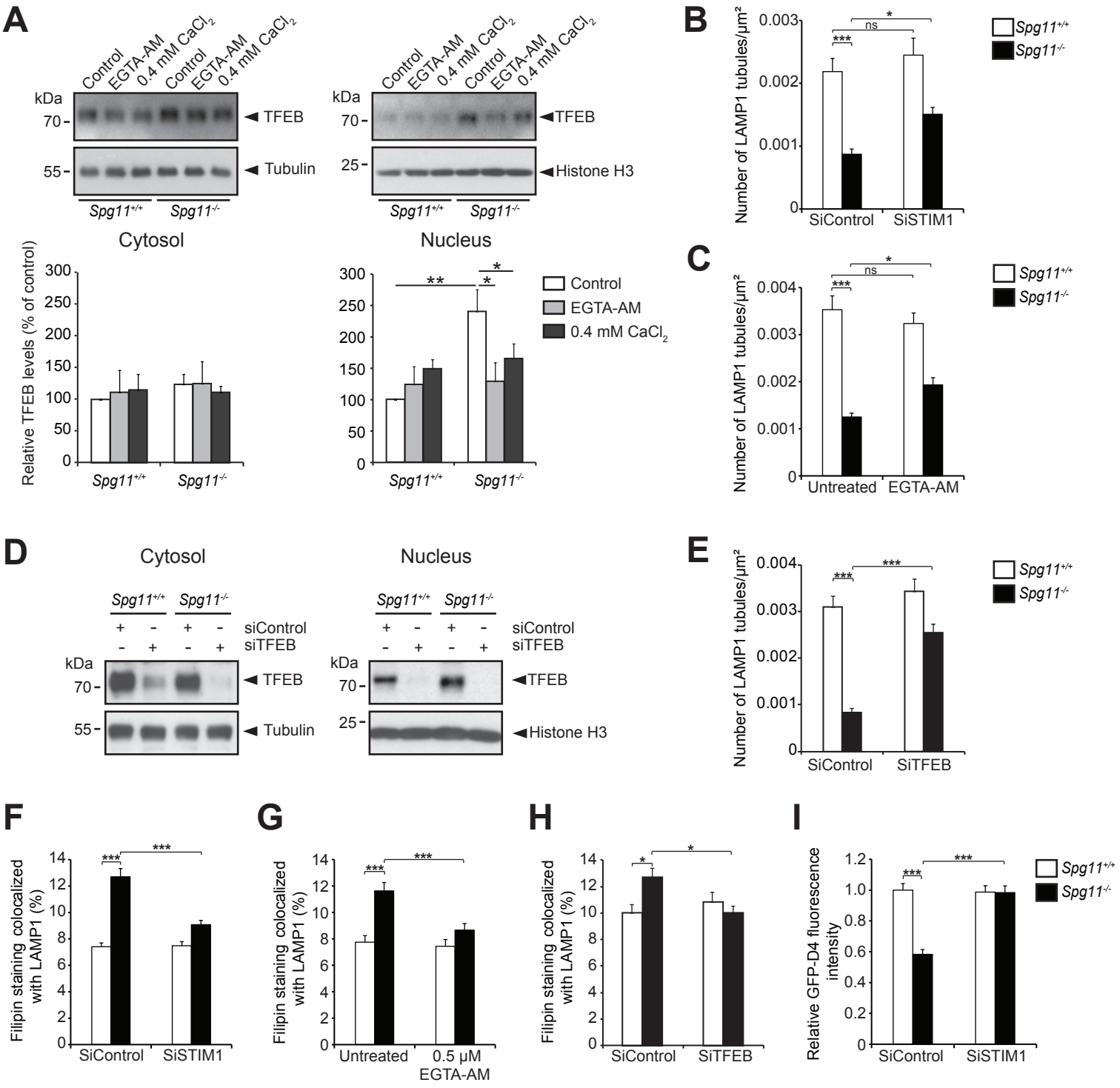

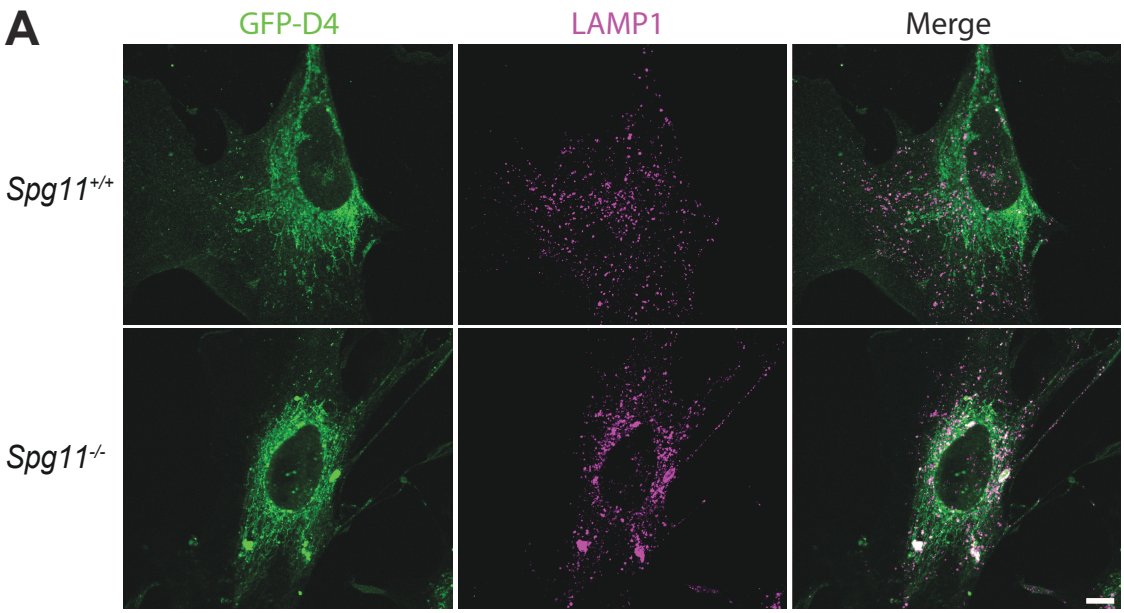

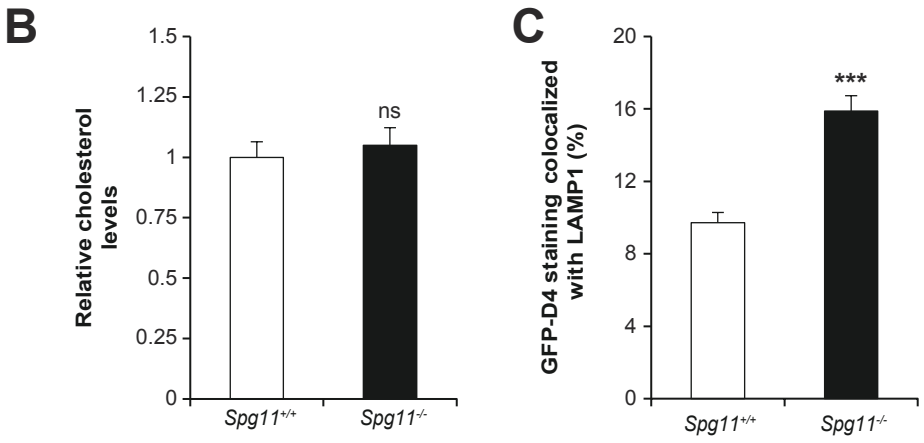

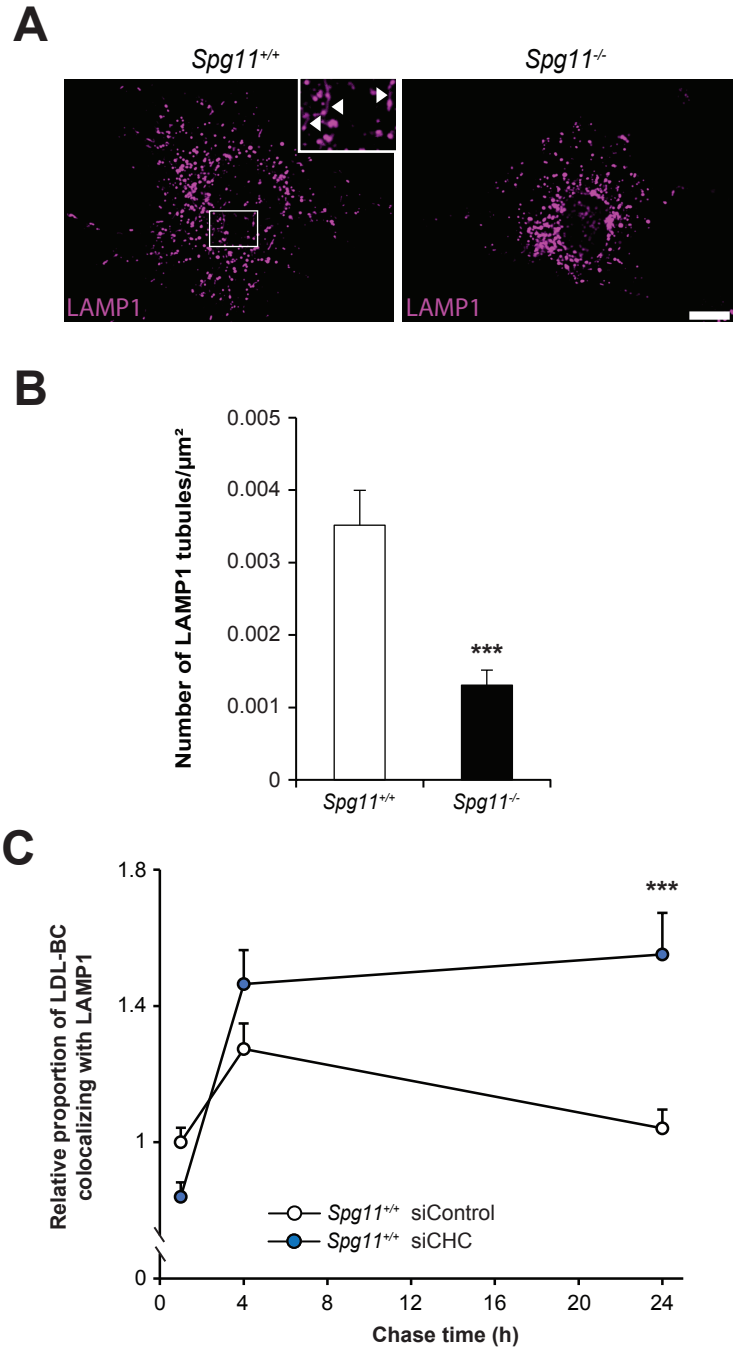

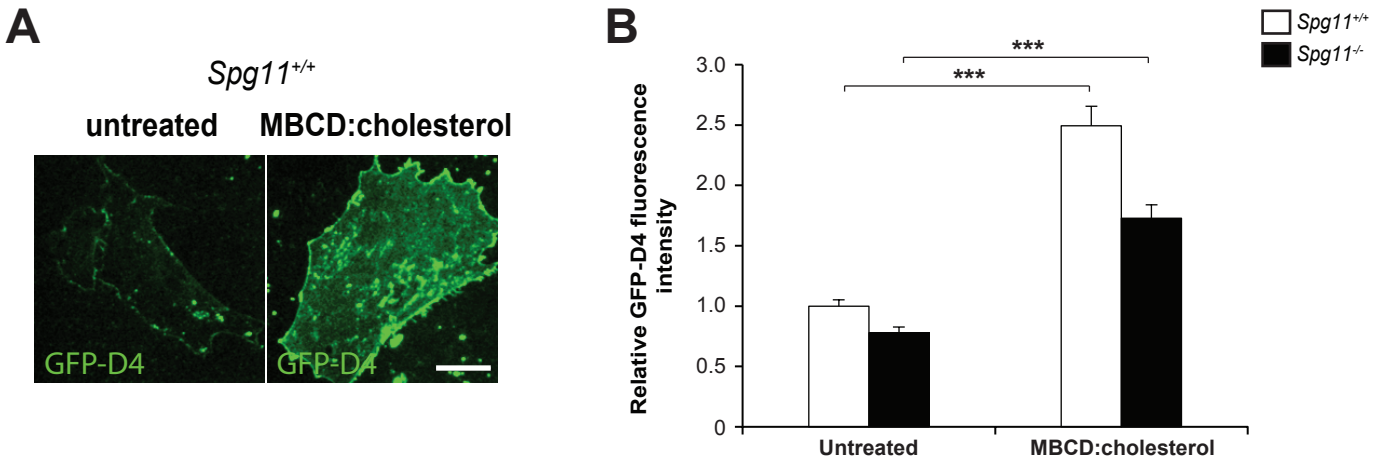

Boutry et al. Sup figure 4

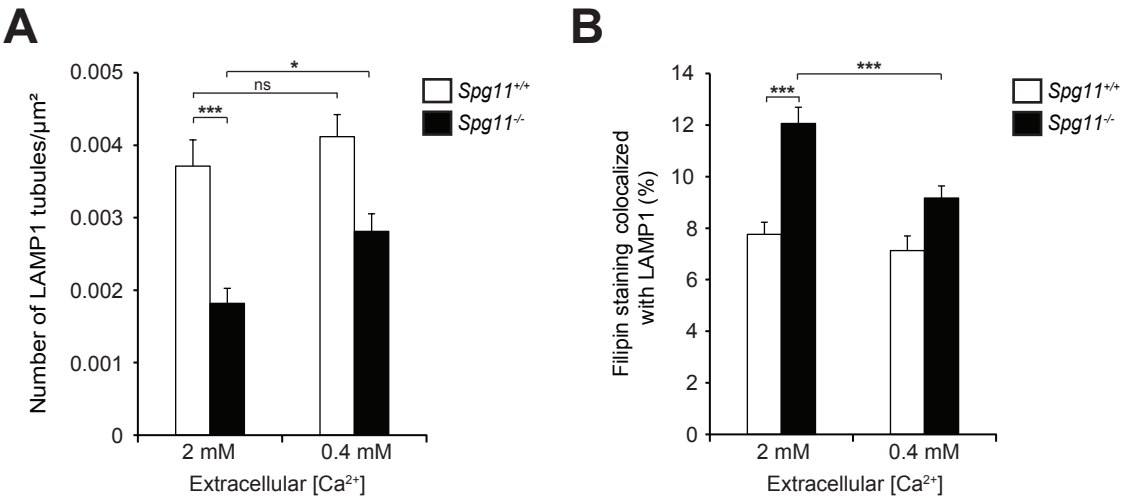

Boutry et al. Sup figure 5